Analysis of a Swimming Micro Robot

Gábor Kósa and Moshe Shoham
Faculty of Mechanical Engineering
Technion, Israel Institute of Technology
Technion City, 32000 Haifa, Israel
mekosha@tx.technion.ac.il

Menashe Zaaroor
Department of Department of Neurosurgery Haifa, Israel
Rambam Medical Center
Haifa, Israel
m_zaaroor@rambam.health.gov.il

***Abstract* – This paper models, analyzes and optimizes a novel swimming method for a swimming micro robot. The propulsion is achieved by creating a traveling wave in an elastic tail made of piezo-electric actuators. The novel swimming method was analyzed analytically by solving the coupled elastic/fluidic problem. The parameters that influence swimming were identified and optimized. It was found that under the extreme size limitations a tail manufactured by current MEMS technology is able to swim at the order of several cm/sec in water.**

Index Terms* – *Micro Robot, Coupled* elastic/fluidic *Analysis, Swimming Robot.

I. Introduction

Propulsion of micro-organisms has longed been studied using techniques of the field of low Reynolds number hydrodynamics (i.e. viscous flow, or Stokes flow) [1], [2]. Such studies define the motion of swimming object as a boundary condition problem and analyze the propulsion velocity, force, torque and consumed power the flow creates. The actuators that creates the motion are much less understood.

Recently, there have been several studies that designed small robots that are able to swim [3-7]. Such studies showed that it is possible to create swimming robots in the order of *1 [cm]*.

The present investigation suggests a new concept of a swimming microrobot for medical use, illustrated in Fig. 1. The micro-robots main components are: the payload, the power source and the propelling (and steering) actuators.

In an earlier paper, [8], the actuating tail consists of three piezo-electric micro-actuators (See Fig. 2) was described. In this article we analyze and optimize the actuators and show that with such an actuator a propelling velocity of the order of *10 [mm/s]* is achievable.

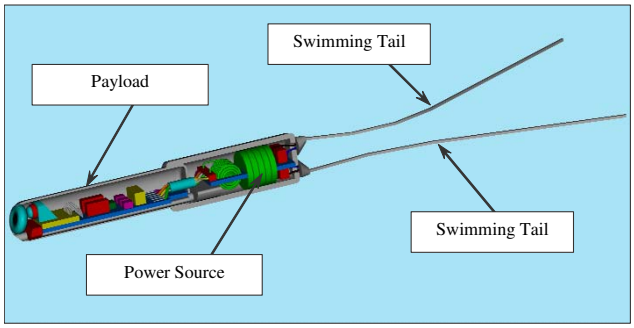

Fig. 1: Illustration of an un-tethered swimming micro-robot.

II. Propulsion Model

Fig. 1 illustrates the concept of a micro-robot propelled by elastic tails. Each tail is actuated by 3 piezoelectric actuators that are modeled as Euler-Bernoulli beam. A short description of the modeling method that was used to solve the elastic-fluidic problem is given next (further details on the model is given in [8]). The beam is divided into three parts each part is described by a distributed variables, $w_i(x,t)$, (See Fig. 2) defined as follows:

$$\begin{aligned} m_1\frac{\partial^2 w_1(x,t)}{\partial t^2}+c_1\frac{\partial w_1(x,t)}{\partial t}+\hat{\mathcal{K}}_1\frac{\partial^4 w_1(x,t)}{\partial x^4}&=0\forall x=[0,\alpha_1 L]\\ m_2\frac{\partial^2 w_2(x,t)}{\partial t^2}+c_2\frac{\partial w_1(x,t)}{\partial t}+\hat{\mathcal{K}}_2\frac{\partial^4 w_2(x,t)}{\partial x^4}&=0\forall x=[\alpha_1 L,\alpha_2 L]\\ m_3\frac{\partial^2 w_3(x,t)}{\partial t^2}+c_3\frac{\partial w_1(x,t)}{\partial t}+\hat{\mathcal{K}}_3\frac{\partial^4 w_3(x,t)}{\partial x^4}&=0\forall x=[\alpha_1 L,L]\end{aligned} \quad (1)$$

where: $m_i=\sum_{j=1}^{n}\rho_{ij}A_{ij}$ is the distributed mass;

$\hat{\mathcal{K}}_i=\sum_{j=1}^{n}Y_j[(1+\xi_j)I_j+A_jZ_j^2]$ is the stiffness coefficient, with

Y_j is the Young modulus of the *j*'-th layer;

I_j is the cross section inertia of the *j*'-th layer;

A_j is the cross section area of the *j*'-th layer;

Z_j is distance from the neutral axes of the *j*'-th layer;

ξ_j is correction term due to the weakening of the electric field applied on the piezoelectric layers by the cross coupling. (For further details see [9]);

$c_i=\frac{2\mu\kappa K_1(\kappa a_i)((K_2(\kappa a_i)K_0(\kappa a_i)-K_1^2(\kappa a_i))\kappa a_i-4K_1(\kappa a_i)K_2(\kappa a_i)}{((K_2(\kappa a_i)+K_0(\kappa a_i))K_1^2(\kappa a_i)-2K_0^2(\kappa a_i)K_2(\kappa a_i)\nu))\kappa a_i+2K_2(\kappa a_i)K_0(\kappa a_i)K_1(\kappa a_i)}$ is the damping coefficient based modified Bessel functions of the (κ is the wave number and a is the radius of the tail) in viscous fluid assuming that the flow around the tail is a Stokes flow and the amplitude of the travelling wave is small, i.e. the deformed cross section of the tail remains circular [10].

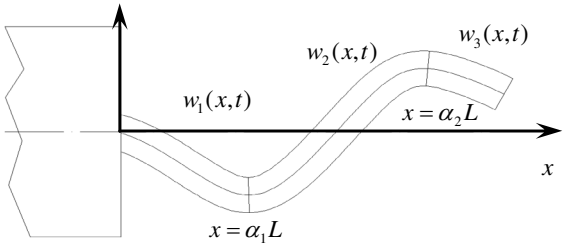

Fig. 2: The tail's three sections.

The boundary conditions (BC) of the beam are clamped at $x=0$ and free at $x=L$:

$$\begin{array}{ll} @\ x=0 & @\ x=L \\ w_1(0,t)=0 & M_3(L,t)=0 \\ \dfrac{\partial w_1(0,t)}{\partial x}=0 & \dfrac{\partial M_3(L,t)}{\partial x}=0 \end{array} \quad (2)$$

The continuity conditions (CC) between the elastic fields are:

$$\begin{array}{ll} @\ x=\alpha_1 L & @\ x=\alpha_2 L \\ w_1(\alpha_1 L,t)=w_2(\alpha_1 L,t) & w_2(\alpha_1 L,t)=w_3(\alpha_1 L,t) \\ \dfrac{\partial w_1(\alpha_1 L,t)}{\partial x}=\dfrac{\partial w_2(\alpha_1 L,t)}{\partial x} & \dfrac{\partial w_2(\alpha_2 L,t)}{\partial x}=\dfrac{\partial w_3(\alpha_2 L,t)}{\partial x} \\ M_1(\alpha_1 L,t)=M_2(\alpha_1 L,t) & M_2(\alpha_2 L,t)=M_3(\alpha_2 L,t) \\ \dfrac{\partial M_1(\alpha_1 L,t)}{\partial x}=\dfrac{\partial M_2(\alpha_1 L,t)}{\partial x} & \dfrac{\partial M_2(\alpha_2 L,t)}{\partial x}=\dfrac{\partial M_3(\alpha_2 L,t)}{\partial x} \end{array} \quad (3)$$

Following [9], the moment M_i in a piezoelectric layered beam is calculated as follows:

$$M_i(x,t)=-\hat{\mathcal{K}}_i\frac{\partial^2 w_i(x,t)}{\partial x^2}-\mathcal{M}_{Ei}(t)\ \forall i=1,2,3 \quad (4)$$

$\mathcal{M}_{Ei}(t)$ are the moments that are created in the beam by the electric field.

The system variables $w_i(x,t)$ is converted to $z_i(x,t)$ to homogenize the boundary and continuity conditions. The general solution of $z_i(x,t)$ is obtained by the method of separation of variables as follows:

$$z_i(x,t)=\sum_k^{\infty}\phi_{i,k}(x)f_k(t)\ \forall i=1,2,3 \quad (5)$$

where: $f_k(t)$ - are the time functions of the variable separation. This function is the same in the different elastic fields along the tail.

$\phi_{i,k}(x)$ - are the shape modes of the system.

The modes differ at each elastic field, but the continuity conditions ensure that they create a smooth spatial function along the three parts of the beam.

By substituting the general solutions, (5), into the BC and CC one can find the natural frequencies and the mode shapes of the beam. Fig. 3 illustrates the first 4 modes of the tail ($m_i=m;\mathcal{K}_i=\mathcal{K}$).

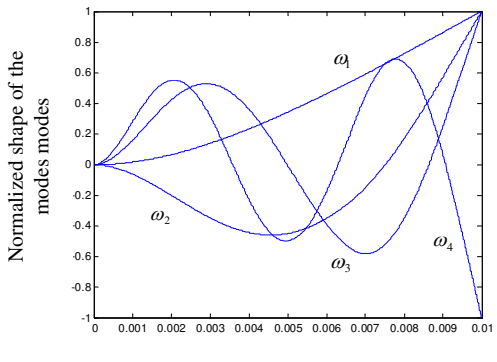

Fig. 3: The beams' modes.

The modes illustrated in Fig. 3 are the solution of the shape mode function, $\phi_{i,k}(x)$. Substituting the shape mode functions into the field equations results a set of time dependent ODE's defined in equation 6:

$$\begin{aligned} &\ddot{f}_k(t)+2\zeta_{1k}\omega_k\dot{f}_k(t)+\omega_k^2 f_k(t)=\frac{Cp_k^{(1)}}{\hat{\mathcal{K}}_1}\left(\ddot{\mathcal{U}}_{E1}(t)+2\zeta_{1k}\omega_k\dot{\mathcal{U}}_{E1}(t)\right) \\ &\ddot{f}_k(t)+2\zeta_{2k}\omega_k\dot{f}_k(t)+\omega_k^2 f_k(t)=\frac{Cp_k^{(1)}}{\hat{\mathcal{K}}_1}\left(\ddot{\mathcal{U}}_{E1}(t)+2\zeta_{2k}\omega_k\dot{\mathcal{U}}_{E1}(t)\right) \\ &+\frac{Cp_k^{(2)}}{\hat{\mathcal{K}}_2}\left(\ddot{\mathcal{U}}_{E2}(t)+2\zeta_{2k}\omega_k\dot{\mathcal{U}}_{E2}(t)\right) \\ &\ddot{f}_k(t)+2\zeta_{3k}\omega_k\dot{f}_k(t)+\omega_k^2 f_k(t)=\frac{Cp_k^{(1)}}{\hat{\mathcal{K}}_1}\left(\ddot{\mathcal{U}}_{E1}(t)+2\zeta_{3k}\omega_k\dot{\mathcal{U}}_{E1}(t)\right) \\ &+\frac{Cp_k^{(2)}}{\hat{\mathcal{K}}_2}\left(\ddot{\mathcal{U}}_{E2}(t)+2\zeta_{3k}\omega_k\dot{\mathcal{U}}_{E2}(t)\right) \\ &+\frac{Cp_k^{(3)}}{\hat{\mathcal{K}}_3}\left(\ddot{\mathcal{U}}_{E3}(t)+2\zeta_{2k}\omega_k\dot{\mathcal{U}}_{E3}(t)\right)\forall k=1,2,..\infty \end{aligned} \quad (6)$$

$Cp_k^{(i)}$ - is a constant derived by the decomposition of the polynomial $p_i(x)$ to the k-th shape function $\phi_k(x)$.

The contribution of each moment, $\mathcal{M}_{Ei}$, was found by by Laplace transformation of (6). The time functions $g_k(t)$, are found from the transfer matrix defined below:

$$\begin{aligned} g_k=&-\frac{Cp_k^{(1)}d_1V_1}{\hat{\mathcal{K}}_1}\left(1+\frac{s(s+2\zeta_{1k}\omega_k)}{s^2+2\zeta_{1k}\omega_k s+\omega_k^2}+\frac{s(s+2\zeta_{2k}\omega_k)}{s^2+2\zeta_{2k}\omega_k s+\omega_k^2}+\frac{s(s+2\zeta_{3k}\omega_k)}{s^2+2\zeta_{3k}\omega_k s+\omega_k^2}\right) \\ &-\frac{Cp_k^{(2)}d_2V_2}{\hat{\mathcal{K}}_2}\left(1+\frac{s(s+2\zeta_{2k}\omega_k)}{s^2+2\zeta_{2k}\omega_k s+\omega_k^2}+\frac{s(s+2\zeta_{3k}\omega_k)}{s^2+2\zeta_{3k}\omega_k s+\omega_k^2}\right) \\ &-\frac{Cp_k^{(3)}d_2V_2}{\hat{\mathcal{K}}_2}\left(1+\frac{s(s+2\zeta_{3k}\omega_k)}{s^2+2\zeta_{3k}\omega_k s+\omega_k^2}\right)\forall k=1,2,..\infty \\ \mathcal{M}_{Ei}=&\,d_iV_i \end{aligned} \quad (7)$$

where: $w_i(x,t)=\sum_k^{\infty}\phi_{i,k}(x)g_k(t)\ \forall i=1,2,3$

This expression can be simplified by assuming that each part of the tail has the same cross section. In this case:

$$\begin{aligned} g_k=&-\frac{d}{\hat{\mathcal{K}}}\left(Cp_k^{(1)}V_1\left(\frac{4s^2+8\zeta_k\omega_k s+\omega_k^2}{s^2+2\zeta_k\omega_k s+\omega_k^2}\right)+Cp_k^{(2)}V_2\left(\frac{3s^2+6\zeta_k\omega_k s+\omega_k^2}{s^2+2\zeta_k\omega_k s+\omega_k^2}\right)+\right. \\ &\left.+Cp_k^{(3)}V_3\left(\frac{2s^2+4\zeta_k\omega_k s+\omega_k^2}{s^2+2\zeta_k\omega_k s+\omega_k^2}\right)\right)\forall k=1,2,..\infty \end{aligned} \quad (8)$$

where $d_j=\sum_i z_i Y_i b_i d_i$, $d_1=d_2=d_3=d$, $\hat{\mathcal{K}}_1=\hat{\mathcal{K}}_2=\hat{\mathcal{K}}_3=\hat{\mathcal{K}}$, and $\zeta_{1k}=\zeta_{2k}=\zeta_{3k}=\zeta_k$.

Equation (7-8) completes the model of the tail and gives the expression of the dynamic response of the tail to input voltage, $V_i(t)$ exserted on the piezoelectric actuators.

It should be mentioned that this model is based on the Euler-Bernoulli beam model, and Taylor fluidic model. For the swimming micro-robots those assumptions are accurate enough since piezoelectric actuators are not able to create large tail deformations.

Once we have the relation between the input model and the tail behaviour, the question is what should be the input voltages in order to create swimming. In viscous flows described by the Stokes equation one has to create a travelling wave. The desired motion of the neutral axis of the tail should be as follows:

$$w(x,t) = b\sin\kappa(x-Ut) = b(\sin\kappa x\cos\kappa Ut - \cos\kappa x\sin\kappa Ut) = \\ = \sum_{k=1}^{\infty}(Cs_k\cos\kappa Ut - Cc_k\sin\kappa Ut)\phi_k(x) = \sum_{k=1}^{\infty} r_k(t)\phi_k(x) \quad (9)$$

b is the amplitude, κ is wave number and U is the velocity of the travelling wave.

If the swimming tail is divided to m actuators the highest number of controllable modes is also m. Each voltage is defined by: $V_i(t) = V_i\sin(\Omega t + \phi_i)$ (two degrees of freedom $V_i;\phi_i$). Each desired time functionhas the form of $r_k(t) = Cs_k\cos\kappa Ut - Cc_k\sin\kappa Ut$ (two degrees of freedom $Cs_i;Cc_i$). Clearly each actuator can apply one voltage i.e. each actuator can define a single time function and by it control a single modal function.

Using the transfer matrix (9) one can find the desired phases and magnitudes for the different input voltages to create a full cycle of a traveling wave shown in Figs. 4a – 4g.

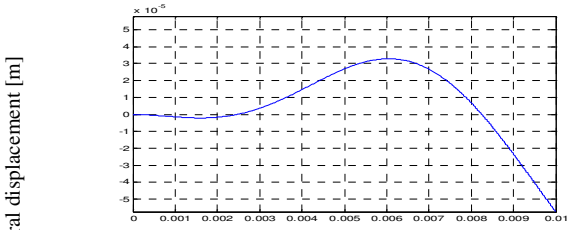

Fig. 4a: The tails displacement at t=0[sec].

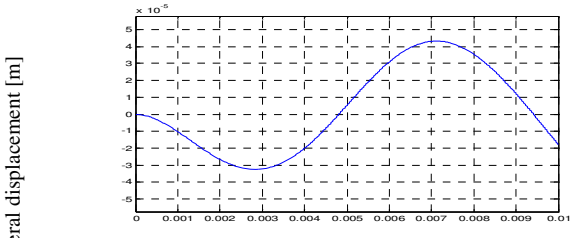

Fig. 4b: The tails displacement at t=π/3/Ω[sec].

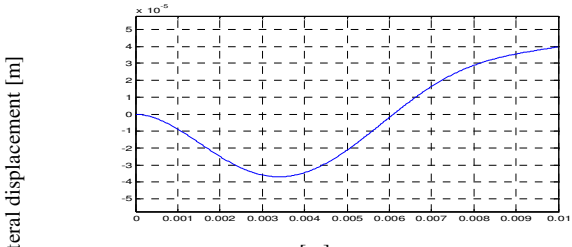

Fig. 4c: The tails displacement at t=2π/3/Ω[sec].

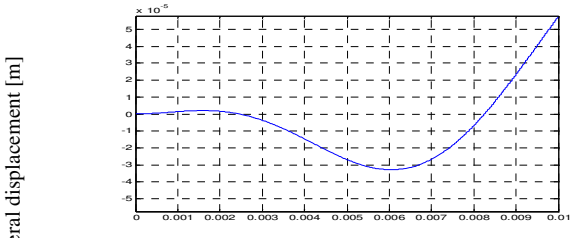

Fig. 4d: The tails displacement at t=π/Ω[sec].

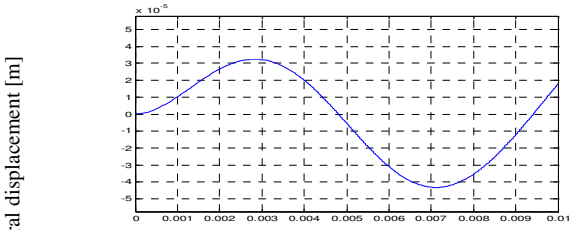

Fig. 4e: The tails displacement at t=4π/3/Ω[sec].

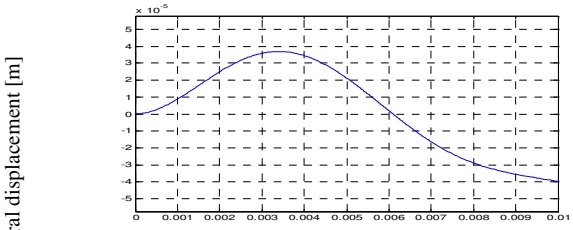

Fig. 4f: The tails displacement at t=5π/3/Ω[sec].

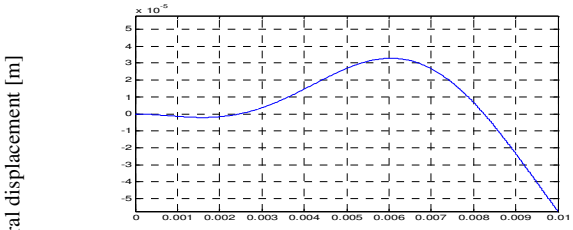

Fig. 4g: The tails displacement at t=2π/Ω[sec].

Notice that the pick of the wave advances along the tail length in contrast to standing waves.

It was shown by Taylor [10] that in Stokes flow the relation between a traveling wave advancing in the tail and the total velocity of the swimming micro-robot is:

$$\frac{U_{MR}}{U} = -\frac{1}{2}\frac{b^2\kappa^2}{\phi(\alpha)}\left(K_0(\kappa a) - \frac{\kappa a}{2}\left(K_1(\kappa a) + \frac{K_0^2(\kappa a)}{K_1(\kappa a)}\right)\right) \quad (10)$$

Were: $\phi(\alpha) = \alpha K_1(\kappa a)\left(\frac{1}{2}\left(1+\frac{K_0(\kappa a)}{K_1(\kappa a)}\right) - \left(\frac{K_0(\kappa a)}{K_1(\kappa a)}\right)^2\right) + K_0(\kappa a)$, $K_i(\kappa a)$ are modified Bessel function of the i-th order.

The propulsion efficiency can also be derived from this equation. The additional drag created by the robots body is not taken into account in this analysis.

III. System Analysis and Optimization

The coupled fluidic-mechanical-electrical model enables the analysis of the influence of the different parameters of the system. One has to determine the wave length and velocity of the desired traveling wave, the shape of the actuator and the influence of the loading parameters such as the viscosity of the surrounding fluid.

The best fit for the decomposition of the traveling wave is $\kappa = 2\pi/L$, i.e. the wavelength of the traveling wave is the length of the tail. Figs. 5 and 6 illustrates the approximation by three and four modal functions, $\phi_k(x)$, of the desired trigonometric functions: $\sin(\kappa x + \phi_C)$ and $\cos(\kappa x + \phi_C)$ functions. ϕ_C is a constant angle that is added to improve the fitting and it's value is 76.78°.

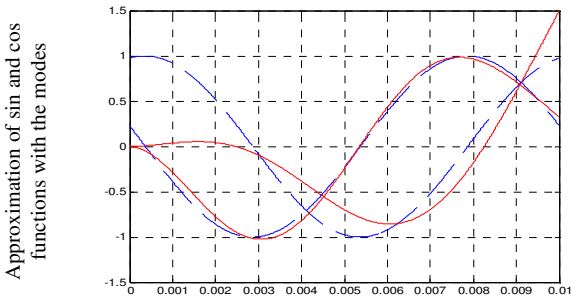

Fig. 5: Approximation of $\sin \kappa x$ and $\cos \kappa x$ functions (blue lines) by three modes of the tail (red lines).

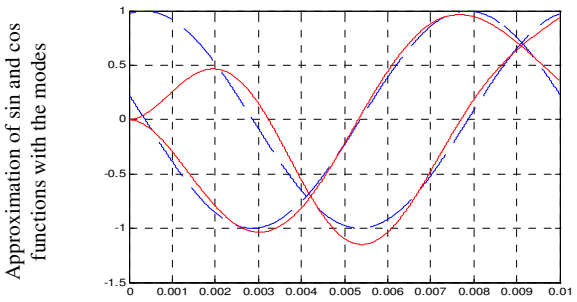

Fig. 6: Approximation of $\sin \kappa x$ and $\cos \kappa x$ functions (blue lines) by four modes of the tail (red lines).

One can observe that the more modal functions are used, the better the fit of the approximated trigonometric functions. The disadvantage is that more modal functions need to be controlled, i.e. more actuators are needed, and the system is more complicated.

The influence of the thickness of a tail was shown in an earlier investigation [8]. In piezoelectric micro-actuators, on contrary to macro actuators, the thickness of the piezoelectric layer has also structural importance. The moment created by the piezoelectric layer is scaled to the layer thickness linearly, $\mathcal{M}_{Ei} \alpha O(t_i)$, and the stiffness of the beam is scaled by the third power, $\mathcal{K}_i \alpha O(t_i^3)$. In general, in a piezoelectric bimorph the thinner the piezoelectric layer's thickness the larger the actuators stroke. In a unimorph or any other composite piezoelectric beam one can find what is the best combination of thicknesses to get maximal stroke. For example taking a unimorph actuator made of a PZT layer and a Si layer (See Fig. 7) .

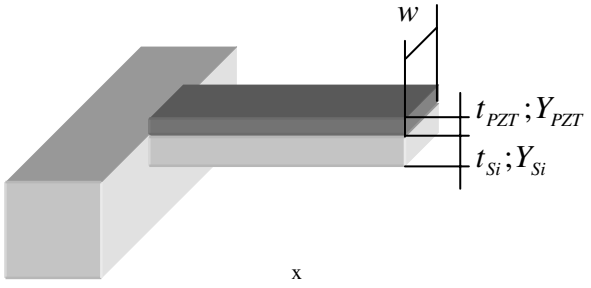

Fig. 7: Illustration of a unimorph made of Si and PZT layers.

The stroke of the actuator is proportional to the term:

$$\frac{\mathcal{M}_{Ei}}{\hat{\mathcal{K}}_i} = \frac{6\alpha\beta(\beta+1)dE}{t_{PZT}(\beta^4\alpha^2+4\beta^3\alpha+6\beta^2\alpha+4\beta\alpha+\xi_{PZT}(\beta\alpha+1)} \quad (11)$$

Where: $\alpha = Y_{Si}/Y_{PZT}; \beta = t_{Si}/t_{PZT}$, E is the electric field on the piezoelectric layer, d is the piezoelectric coefficient and ξ_{PZT} is the cross coupling coefficient.

TABLE I
PHYSICAL PROPERTIES OF THE TAILS LAYERS

Layer	Silicon	PZT
Specific weight [kg/m^3]	2330	7700
Young modulus [GPa] *	141.17	70.05
Piezoelectric coefficient [pC/N] *	-	-230.7
Dialectric constant [nF/N] *	-	15.49
Cross coupling coefficient *k* *	-	0.138

[a]See [9] for details on how those coefficients are calculated.

For the physical properties given in Table 1 the optimal thickness ratio β is $\beta = 0.386$. Fig. 8 illustrates the dependence of the stiffness in the parameter β and the single maxima.

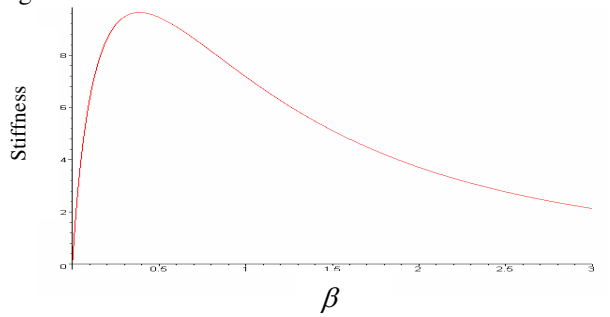

Fig. 8: The stiffness of the Si-PZT beam for different thickness ratios.

An additional parameter that influences the propulsion velocity is the length of each actuator in the tail, i.e. the parameters α_1 and α_2. In the earlier study, [8], the actuators were divided equally, $\alpha_1 = 1/3; \alpha_2 = 2/3$. For a tail defined in Fig. 8 and Si layer thickness of $20\,[\mu\text{m}]$ is the propulsive velocity that was achieved was $U_{MR} = 7.4\,[\text{mm/s}]$. In Fig. 9 we show the propulsive velocity for the parameter range: $\alpha_1 = [0.01, 0.98]; \alpha_2 = [\alpha_1, 0.99]$. One can observe that there is a local maxima at $\alpha_1 = 0.13; \alpha_2 = 0.46$. The propulsive velocity at the maxima is $U_{MR} = 80.87\,[\text{mm/s}]$.

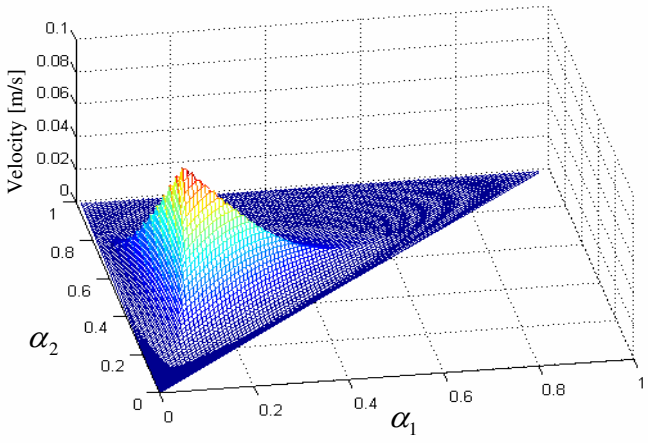

Fig. 9: Propulsion velocity achieved by different actuator configurations.

The reason of such a dramatic increase in the propulsive velocity is the voltage that is applied on each actuator. In the

case of even distribution of actuator lengths, the voltage on each actuator is: $[V_1,V_2,V_3]=[0.771,3.49,10][Volt]$. These voltage amplitudes create a traveling wave along the tail. In the case of actuator lengths of $\alpha_1=0.13;\alpha_2=0.46$, the voltages on $0.1[mm]$ the actuators are $[V_1,V_2,V_3]=[9.93,10,9.75]$. The second actuator configuration takes much better advantage of the applied voltage, hence more energy is entered into the tail the amplitude of the traveling wave is increased and the propulsive velocity is larger. The optimization of the actuator sizes was found with accuracy of $\delta\alpha_i=0.01$ We assume that larger resolution one can achieve $10[Volt]$ voltage on all the actuators.

The actuator distribution is invariant under the total tail length L, or other parameters of the tail (assuming the tail has the same cross section all along). The parameters that influence the actuator distribution are the damping coefficients ζ_k. An under-damped modal function, for example $\zeta_3<1$ causes greater sensitivity at the resonance and different reaction of the tail to the piezo-actuators excitation. Thus the optimization is not global for the total parameter space.

Fig. 10 illustrates the propulsive velocity for the same parameter range as the previous figure. The thickness of the Si layer was increased in this optimization to $60[\mu m]$. In this case the maximal velocity is $U_{MR}=3.84$ [mm/s] and the actuator configuration is: $\alpha_1=0.14;\alpha_2=0.49$ (different from the earlier optimization values).

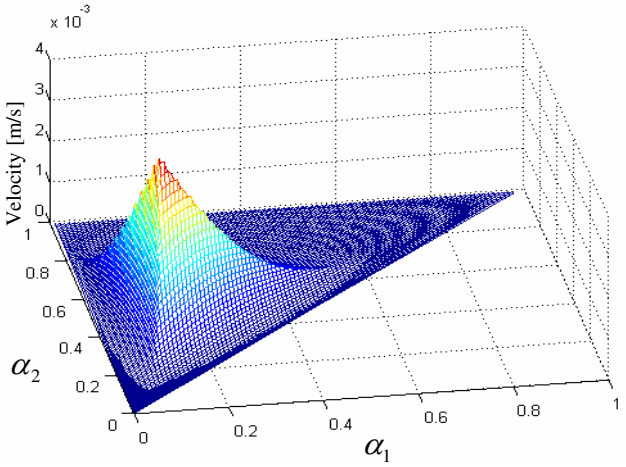

Fig. 10: Propulsion velocity achieved by different actuator configurations.

IV. Conclusions

In conclusion, the propulsion presented here can achieve velocity of the order of 1 [cm/sec] and it is compact and simple to manufacture. The analytical model enables this optimization in comparison to a numerical model in which analysis is more difficult. The increase of the propulsion is achieved by fully taking advantage of the actuator voltages in building the traveling wave.

References

[1] T. Ebefors and G. Stemme (Chief editor M. Gad-El-Hak), *The MEMS handbook*, Chapter 28- Micro-robotics, CRC Press, 2002, pp. 28-1 – 28-42, .

[2] Y. Haga, Y. Tanahashi and M. Esashi, "Small Diameter active catheter using shape memory alloy", *Micro Electro Mechanical Systems (MEMS'98)*, pp.419-424, January 1998.

[3] D.R. Yarborough 3rd, J.C. McAlhany, M.G. Weidner and N. Cooper et al., "Evaluation of the Heidelberg Capsule: Method of Tubeless Gastric Analysis", *American Journal of Surgery*, vol. 117(2), pp. 185-191, February 1969.

[4] T. Fukuda, A. Kawamoto, F. Arai and Matsuura, H.; "Mechanism and swimming experiment of micro mobile robot in water", *IEEE Conference on Robotics and Automation (ICRA'94)*, vol. 1, pp. 814-819, May 1994.

[5] K.B. Yesin, K. Vollmers, and B.J. Nelson., "Analysis and design of wireless magnetically guided microrobots in body fluids" *IEEE Conference on Robotics and Automation (ICRA'04)*, pp. 1333-1338, April 2004.

[6] L. Yawen, R.S. Shawgo, R. Langer, R. and M.J. Cima, "Mechanical testing of gold membranes on a MEMS device for drug delivery ", *2nd Annual International IEEE EMBS-Special Topic Conference on Microtechnologies in Medicine and Biology*, pp. 390-393, May 2002.

[7] S. Guo, Y. Okuda amd K. Asaka, "A novel type of underwater micro biped robot with multi DOF", *IEEE Conference on Robotics and Automation (ICRA'04)*, pp. 4881-4886, April 2004.

[8] G. Kosa, M. Shoham and M. Zaaroor., "Propulsion of a Swimming Micro Medical Robot", *IEEE Conference on Robotics and Automation (ICRA'05)*, pp. 1339-1343, April 2005.

[9] E. Tadmor and G. Kosa, "Electromechanical coupling correction for piezoelectric layered beams", *JMEMS*, vol. 12, pp. 899-906, December 2003.

[10] G.I. Taylor, "The action of waving cylindrical tails in propelling microscopic organisms, *Proceedings of the Royal Society A*, pp. 225-239, 1952.

[11] J. Edd, S. Payen, B. Rubinsky; M.L. Stoller and M. Sitti, "Biomimetic propulsion for a swimming surgical micro-robot", *IEEE/RSJ Intelligent Robotics and Systems Conference*, vol. 3, pp. 2583 – 2588, October 2003.

[12] J.E. Avron, O. Gat and O. Kenneth, " Optimal Swimming at Low Reynolds Numbers", *Physical Review Letters*, vol. 93, pp. 186001/1-4, 2004.